Implementation of Computational Contact Analysis in Geotechnical Engineering

Daqing Xu[1(✉)], Luis G. Vasquez[2], and William M. Isenhower[1(✉)]

[1] Ensoft, Inc, 3003 West Howard Lane, Austin 78728, TX, USA
(5l2) 244-6464lcra@ensoftinc.com
[2] Ensoft, Inc./Lymon C. Reese and Associates, Inc, 3003 West Howard Lane, Austin 78728, TX, USA

Abstract. Analyses of mechanical interactions between soil and structural members in geotechnical engineering are long-standing challenges in the design of piles, foundations, retaining walls, and culverts. Due to the high nonlinearity of these problems, numerical solutions using finite element method (FEM) and finite differences are dominant in engineering practice. In this paper, a detailed procedure of FEM implementation is presented to solve 2D frictional interaction problems with finite sliding. This presentation starts from the geometrically exact theory to express the kinematics of contact, virtual work equation and linearization in the local convective coordinate system. Formulations of the contact tangent stiffness become straightforward and easy to understand. Tangential behavior is simulated by the regularized Coulomb friction law and constraints are enforced by the penalty approach. If linear finite elements are used, local smoothing is essential to improve convergence performance. Two applications in geotechnical engineering are presented to demonstrate the capabilities of this implementation.

Keywords: Node-to-segment · Penalty · Frictional · Finite element
Covariant coordinate

1 Introduction

Soil-structure interaction problems are frequently encountered in geotechnical engineering, such as interactions between soil-culvert, soil-retaining wall, soil-pile, soil-concrete dam, etc. Contact states can be “in contact” or “open” in the normal direction, and “sticking” or “sliding” in the tangential direction. These problems are highly nonlinear in nature and closed-form solutions are only available for few cases. Most solutions have to be obtained by numerical approaches like the finite element method (FEM). After more than thirty years of effort, a framework for analysis of contact problems has been well established and general-purpose FEM programs are available to solve complicated contact problems in today’s engineering practice. However, due to complexity in theory and significant difficulties in the development of programs, availability of FEM software to solve interaction problems in geotechnical engineering is still limited.

M.-C. Weng et al. (eds.), *Current Geotechnical Engineering Aspects of Civil Infrastructures*, Sustainable Civil Infrastructures,
https://doi.org/10.1007/978-3-319-95750-0_5

Using FEM to solve soil-structure interactions can trace its origin to the early 1960s. Goodman [1] developed an interface element with zero thickness to simulate the interface behavior in rock. Desai and Zaman [2] proposed a thin-layer interface element to simulate rock joints. In these methods, node-to-node contact status must be maintained. This approach has the benefit of convenient implementation. However, when the interface has finite sliding this approach can have major difficulties because node-to-node contact status cannot be maintained.

In solid mechanics, versatile approaches have been developed to solve general multi-body contact problems. References [3–5] are early advances in this field where Lagrange multiplier method or the penalty method is employed to apply contact constraints. The interface can be frictionless or frictional. Among various approaches, the penalty method has attracted more interest. Although impenetrability (non-penetration) is only approximately satisfied, the penalty approach has advantages of good convergence performance and convenient incorporation into current FE codes. Kikuchi and Oden [6] have discussed theoretical formulations and implementation of penalty approach for frictionless and frictional contacts. Other early references related with the penalty approach can be found in [7, 8].

In linearization of the variational equation, the *direct approach* is popular in publications in which linearization is applied to discrete configurations. However, procedures of linearization to generate a consistent stiffness matrix are usually complicated and difficult to understand. An alternative approach is known as *covariant approach*. Kinematics of contact bodies are expressed in local coordinate system. Linearization is applied to the weak form of the continuous version to obtain the tangent contact stiffness in a covariant form. This approach involves many covariant operations; however, formulations of contact stiffness are straightforward and more understandable. Details of this approach can be found in [9, 10].

In this work, implementation of computational contact analysis to solve problems in geotechnical engineering is introduced. After the introduction section, the kinematics of contact, virtual work and tangent stiffness in the covariant form are described. Following is the section about finite element discretization, calculation of closest point projection (CPP) and other issues related with program development. In the last section, two applications in geotechnical engineering are presented.

2 Kinematics of Contact

The configuration of a contact problem between two solid bodies is depicted in Fig. 1. We use the symbols Ω^A and Ω^B to denote solid bodies and Γ_u, Γ_σ, and Γ_c to denote the displacement boundary, force boundary and contact boundary respectively. The terminology "master-slave" is adopted to distinguish Ω^A from Ω^B. The "master" body has a larger Young's modulus or stiffer material. In geotechnical engineering, structures are usually concrete or steel. Thus, the "master" title is assigned to the structure and "slave" is assigned to the soil generally. In the "node-to-segment" approach discussed in this work, the terminology "contact pairs" is used to describe the interaction on the interface. Each contact pair includes one "slave" point from the slave body and one

piece of the "master" 2D curve or 3D surface as depicted in Fig. 2. The local coordinate system is defined on the master body side. We denote the position vector of the slave point by $\boldsymbol{r}_s$ and the master surface by the position vector

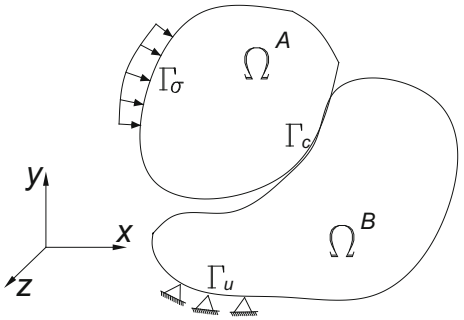

Fig. 1. Configuration of two-body contact problem

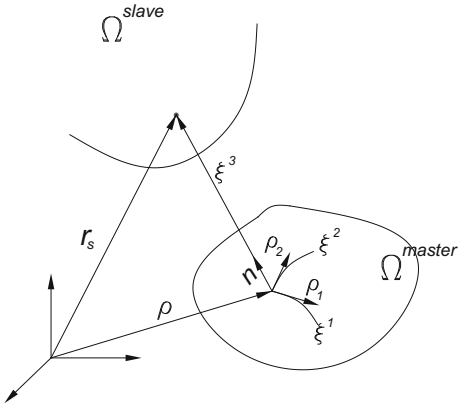

Fig. 2. Local coordinate system and closest point projection

$$\boldsymbol{\rho} = \boldsymbol{\rho}\left(\xi^1, \xi^2\right) \tag{1}$$

where ξ^1, ξ^2 are local coordinates. When contact happens, impenetrability should be satisfied so that the slave point has zero gap to its projection on the master surface. The procedure to find the "Closest Point Projection (CPP)" can be expressed as

$$\min||\boldsymbol{r}_s - \boldsymbol{\rho}(\xi^1, \xi^2)|| \tag{2}$$

The normal gap ξ^3 between the slave point and its CPP is computed using

$$\boldsymbol{r}_s = \boldsymbol{\rho}(\xi^1, \xi^2) + \xi^3 \mathbf{n} \tag{3}$$

where $\mathbf{n}$ is the outward unit norm on the master surface.

3 Normal Contact

In the normal direction, a slave point may have a positive gap (separation) with zero contact traction, or touch the master surface with zero gap and non-zero contact traction. This geometrical constraint can be described by the Kuhn-Tucker condition by measurement of ξ^3 (see Fig. 2 for definition of ξ^3).

$$\begin{cases} \xi^3 > 0, & no\ contact\ and\ t_N = 0 \\ \xi^3 \leq 0, & in\ contact\ and\ t_N = \int_N \xi^3 \end{cases} \tag{4}$$

where t_N is the normal contact traction and ϵ_N is the normal penalty parameter. One may note that t_N is negative in Eq. 4 and penetration does not vanish when contact occurs. Although the penalty approach satisfies the non-penetration constraints approximately, results with good engineering accuracy are still available when appropriate penalty parameters are used. In theory, ϵ_N is recommended to be set as large as possible.

4 Tangential Contact

A frictional contact is more common than a frictionless one. The interface of soil-structure interactions is often rough and tangential friction stresses may play an important role in analysis. However, interface friction is a complicated phenomenon that involves normal pressure, roughness of the interface, temperature and relative velocity, etc. Among various approaches, the Coulomb friction law is widely adopted. Classical Coulomb law assumes that there is no relative tangent displacement when the tangential force is smaller than a threshold value. Once sliding starts, the tangent friction force is linearly proportional to the normal pressure. The classical Coulomb law has implementation difficulties due to the sudden change from zero relative displacement to sliding. Regularized Coulomb friction law is recommended which allows a small relative motion before sliding.

Tangential contact status should be distinguished as “sticking” or “sliding”. As an analogy to elasto-plasticity, we define the tangential sliding function as

$$\Phi = |\boldsymbol{t}_T| - \mu t_N \tag{5}$$

where μ is the coefficient of interface friction and $\boldsymbol{t}_T$ is the tangential contact traction. Equation 5 has the difficulty of differentiability and regularization is necessary.

We follow the same regularization as in [14], and rewrite the relative sliding velocity $\mathbf{v}_r$ in the regularized form:

$$\frac{d\boldsymbol{t}_T}{dt} = -\epsilon_T \mathbf{v}_r \tag{6}$$

where ϵ_T is the tangential penalty parameter.

The left part in Eq. 6 is the time derivative of the tangent contact tractions. For static problems in 2D assumptions, local coordinates reduce to one parameter and we can use an increment of displacement $\Delta\xi^1$ to replace the rate form of Eq. 6. Thus,

$$T^1_{n+1} - T^1_n = -\epsilon_T \Delta\xi^1 = -\epsilon_T\left(\xi^1_{n+1} - \xi^1_n\right) \tag{7}$$

The subscript n and $n + 1$ represent consecutive load increments. At initial conditions, $T^1_0 = 0$, $\xi^1_0 = \xi_c$, where ξ_c is the initial Closest Point Projection.

Determination of tangential contact status of a slave point under the $n + 1$ load increment has the following steps:

- Calculate trial of $\boldsymbol{t}_T$. In case of a 2D problem, trial of T^1 at $n + 1$ load increment is calculated as

$$T^{1,trial}_{n+1} = -\epsilon_T \Delta\xi^1 \tag{8}$$

- Real tangential traction is determined by the returning mapping algorithm.

$$T^1 = \begin{cases} T^{1,trial}_{n+1} \; if \left|T^{1,trial}_{n+1}\right| \le \frac{\mu|t_N|}{|\boldsymbol{\rho}_1|} & keepsticking \\ -\frac{\Delta\xi^1}{\left|\Delta\xi^1\right|}\frac{\mu|t_N|}{|\boldsymbol{\rho}_1|} \; if \left|T^{1,trial}_{n+1}\right| \ge \frac{\mu|t_N|}{|\boldsymbol{\rho}_1|} & changetosliding \end{cases} \tag{9}$$

If sliding occurs, update closest point projection ξ_c using

$$\xi_c = \xi^1_{n+1} - \frac{\Delta\xi^1}{\left|\Delta\xi^1\right|}\frac{\mu|t_N|}{\epsilon_T|\boldsymbol{\rho}_1|} \tag{10}$$

where $\boldsymbol{\rho}_1$ is the first derivative $\boldsymbol{\rho}_1 = \frac{\partial\boldsymbol{\rho}}{\partial\xi^1}$

5 Weak Equilibrium

On the contact interface, active contact tractions between Ω^A and Ω^B have the same value, but directions are inverted. Therefore, it is possible to write the total contact traction $\boldsymbol{t}_c$ acting on the slave point as

$$\boldsymbol{t}_c = t_N \mathbf{n} + \boldsymbol{t}_T = t_N \mathbf{n} + T^i \boldsymbol{\rho}_i \tag{11}$$

Assuming the interface deformation to be small and problems to be static, the virtual work of the two-body contact problem has the following form

$$\begin{aligned} &\int_{\Omega^A} \left[\boldsymbol{\sigma}^A : \nabla \delta \boldsymbol{u} - \boldsymbol{b}^A \cdot \delta \boldsymbol{u}\right] d\Omega + \int_{\Omega^B} \left[\boldsymbol{\sigma}^B : \nabla \delta \boldsymbol{u} - \boldsymbol{b}^B \cdot \delta \boldsymbol{u}\right] d\Omega \\ &\quad - \int_{\Gamma_\sigma} \boldsymbol{t}_\sigma^A \cdot \delta \boldsymbol{u} d\Gamma_\sigma - \int_{\Gamma_\sigma} \boldsymbol{t}_\sigma^B \cdot \delta \boldsymbol{u} d\Gamma_\sigma - \int_{\Gamma_c} \boldsymbol{t}_c \cdot (\delta \boldsymbol{r}_s - \delta \boldsymbol{\rho}) d\Gamma_c \end{aligned} \tag{12}$$

where $\delta \boldsymbol{u}$ is the virtual displacement and $\boldsymbol{b}$ is the body force.

The last component in Eq. 12 is the virtual work δW^c contributed from the contact tractions. In 2D conditions, δW^c can be simplified to follows:

$$\delta W^c = \delta W_N^c + \delta W_T^c = \int \left[t_N \delta \xi^3 + T^1 (\boldsymbol{\rho}_1 \cdot \boldsymbol{\rho}_1) \delta \xi^1\right] d\Gamma_c \tag{13}$$

6 Linearization

In this section, we focus on linearization of the contact virtual work δW^c only. Since contact analysis is highly nonlinear, an iterative method such as Newton's method is required. Therefore, it is necessary to develop the tangent stiffness of Eq. 13. Operations of the time derivative to Eq. 13 are quite complicated. Thus, this part is omitted in this paper. Interested readers can refer to [9–11] for more detail. Here we only list results after linearization. Assuming the problems are 2D, the normal and tangential contact stiffness have the following formulations:

7 Directional Derivative of the Normal Part

$$\begin{aligned} D_v\left(\delta W_N^c\right) = &\int_s \epsilon_N H\left(-\xi^3\right)(\delta \boldsymbol{r}_s - \delta \boldsymbol{\rho}) \cdot (\mathbf{n} \otimes \mathbf{n})(\mathbf{v}_s - \mathbf{v}) ds \\ &- \int_s \epsilon_N \xi^3 H\left(-\xi^3\right) \left[\delta \boldsymbol{\tau} \cdot (\mathbf{n} \otimes \boldsymbol{\tau})(\mathbf{v}_s - \mathbf{v}) + (\delta \boldsymbol{r}_s - \delta \boldsymbol{\rho}) \cdot (\tau \otimes \mathbf{n}) \frac{\partial \boldsymbol{\tau}}{\partial t}\right] ds \\ &- \int_s \epsilon_N \xi^3 H\left(-\xi^3\right) \kappa (\delta \boldsymbol{r}_s - \delta \boldsymbol{\rho}) \cdot (\boldsymbol{\tau} \otimes \boldsymbol{\tau})(\mathbf{v}_s - \mathbf{v}) ds \end{aligned} \tag{14}$$

where $\mathbf{v}_s = \frac{d\boldsymbol{r}_s}{dt}$ is the absolute velocity of the slave point, $\mathbf{v} = \frac{d\boldsymbol{\rho}}{dt}$ is the velocity of the point with CPP on the master surface, κ is the curvature, and $H(*)$ is the Heaviside function.

Equation 14 has three components as mentioned in Ref. [13]. These components include the primary part, the rotation part and the curvature part sequentially. If deformation at the interface is small, the rotation and curvature parts can be ignored.

Additionally, the curvature part vanishes if linear finite elements are used because the curvature of a straight line is zero.

8 Directional Derivative of the Tangential Part

Contact statuses in the tangential direction are distinguished as "sticking" and "sliding". For the sticking status, linearization has the following result:

$$\begin{aligned} D_v\left(\delta W_T^c\right) = & -\int_s \frac{\epsilon_T}{\boldsymbol{\rho}_1 \cdot \boldsymbol{\rho}_1}(\delta \boldsymbol{r}_s - \delta\boldsymbol{\rho}) \cdot (\boldsymbol{\rho}_1 \otimes \boldsymbol{\rho}_1)(\mathbf{v}_s - \mathbf{v}) ds \\ & -\int_s \frac{T^{real}}{(\boldsymbol{\rho}_1 \cdot \boldsymbol{\rho}_1)^2}\left[(\delta \boldsymbol{r}_s - \delta\boldsymbol{\rho}) \cdot (\boldsymbol{\rho}_1 \otimes \boldsymbol{\rho}_1)\frac{\partial \mathbf{v}}{\partial \xi} + \delta\rho_1(\boldsymbol{\rho}_1 \otimes \boldsymbol{\rho}_1)(\mathbf{v}_s - \mathbf{v})\right] ds \\ & -\int_s \frac{T^{real} h_{11}}{(\boldsymbol{\rho}_1 \cdot \boldsymbol{\rho}_1)^2}(\delta \boldsymbol{r}_s - \delta\boldsymbol{\rho})(\boldsymbol{\rho}_1 \otimes \mathbf{n} + \mathbf{n} \otimes \boldsymbol{\rho}_1)(\mathbf{v}_s - \mathbf{v}) ds \end{aligned} \tag{15}$$

Similar to Eq. 14, the second and third lines in Eq. 15 are the rotation and curvature parts respectively, both of which can be ignored if the contact deformation is small. Obviously, the tangent stiffness for the sticking pair is symmetric if only the primary part of Eq. 15 is used.

For the sliding status, we have the directional derivative of δW_T^c as the following:

$$\begin{aligned} D_v\left(\delta W_T^c\right) = & -\int_s \frac{\epsilon_N \mu \cdot sign\left(T_1^{trial}\right)}{\sqrt{\boldsymbol{\rho}_1 \cdot \boldsymbol{\rho}_1}}(\delta \boldsymbol{r}_s - \delta\boldsymbol{\rho}) \cdot (\boldsymbol{\rho}_1 \otimes \mathbf{n})(\mathbf{v}_s - \mathbf{v}) ds \\ & -\int_s \frac{\mu |t_N| \cdot sign(T^{real})}{(\boldsymbol{\rho}_1 \cdot \boldsymbol{\rho}_1)^{3/2}}\left[(\delta \boldsymbol{r}_s - \delta\boldsymbol{\rho}) \cdot (\boldsymbol{\rho}_1 \otimes \boldsymbol{\rho}_1)\frac{\partial \mathbf{v}}{\partial \xi} + \delta\boldsymbol{\rho}_1(\boldsymbol{\rho}_1 \otimes \boldsymbol{\rho}_1)(\mathbf{v}_s - \mathbf{v})\right] ds \\ & -\int_s \frac{\mu h_{11} \cdot sign(T^{real})}{(\boldsymbol{\rho}_1 \cdot \boldsymbol{\rho}_1)^{3/2}}(\delta \boldsymbol{r}_s - \delta\boldsymbol{\rho})(2\boldsymbol{\rho}_1 \cdot \mathbf{n} + \mathbf{n} \otimes \boldsymbol{\rho}_1)(\mathbf{v}_s - \mathbf{v}) ds \end{aligned} \tag{16}$$

Again, the second and third components in Eq. 16 can be omitted when the contact deformation is small.

h_{11} in Eqs. 15 and 16 is the covariant component of the curvature tensor. The primary part of the tangential stiffness for the sliding pair is non-symmetric as indicated in Eq. 16. Consequently, the global tangent stiffness is also non-symmetric.

9 Finite Element Discretization

In the procedure of finite element discretization, original continuous domains are replaced by finite number of small quadrilateral or triangular elements. In contact analysis, three methods are developed in the discrete level: node-to-node,

node-to-surface, and surface-to-surface. Node-to-node approach is the simplest one, but applications are limited to small sliding cases. Node-to-surface or node-to-segment is applicable to contact problem subjected to finite sliding and large deformations. The only limitation is that the slave body has to be approximated by linear finite elements. The surface-to-surface approach is the latest approach which has no limitation of quadratic approximation. This approach is still under development but represents the direction of computational contact analysis. However, this approach is more complicated than the node-to-surface approach in both theory and programming. In this paper, the node-to-segment approach is employed which is suitable for most contact problems in geotechnical engineering.

The discrete version of a contact pair includes one finite element node from the slave body and one line segment from the master body. In 2D cases, independent coordinates in the local coordinate system reduce to one parameter ξ^1. Let $\boldsymbol{x}_1$ and $\boldsymbol{x}_2$ represent position vectors of the start and end nodes of the master segment (Fig. 3), Closest Point Projection (CPP) has a close form solution as follows:

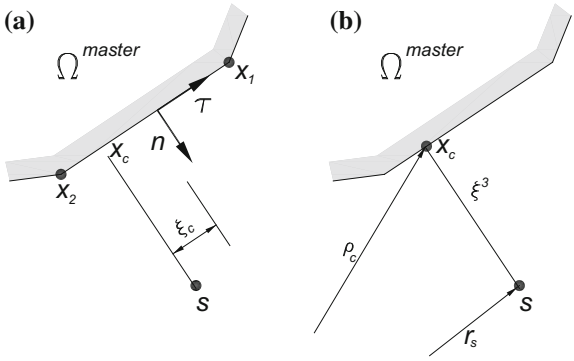

Fig. 3. Depiction of contact pair and location of closest point projection (CPP)

$$\xi_c = \frac{2\boldsymbol{r}_s \cdot (\boldsymbol{x}_2 - \boldsymbol{x}_1) - \boldsymbol{x}_2 \cdot \boldsymbol{x}_2 + \boldsymbol{x}_1 \cdot \boldsymbol{x}_1}{(\boldsymbol{x}_2 - \boldsymbol{x}_1) \cdot (\boldsymbol{x}_2 - \boldsymbol{x}_1)} \tag{17}$$

Points on the master segment can be interpolated by

$$\boldsymbol{\rho}(\xi^1) = \frac{1 - \xi^1}{2}\boldsymbol{x}_2 + \frac{1 + \xi^1}{2}\boldsymbol{x}_1 \tag{18}$$

where $\xi^1 = -1$ at $\boldsymbol{x}_2$ and $\xi^1 = 1$ at $\boldsymbol{x}_1$.

The position vector from the slave point to the master surface is determined by

$$\boldsymbol{r}_s - \boldsymbol{\rho}\left(\xi^1\right) = \begin{bmatrix} -1 & 0 & \frac{1-\xi^1}{2} & 0 & \frac{1+\xi^1}{2} & 0 \\ 0 & -1 & 0 & \frac{1-\xi^1}{2} & 0 & \frac{1+\xi^1}{2} \end{bmatrix} \begin{bmatrix} x_s \\ y_s \\ x_2 \\ y_2 \\ x_1 \\ y_1 \end{bmatrix} = [\mathbf{N}]\{\mathbf{x}\} \tag{19}$$

By means of Eqs. 18 and 19, the tangent stiffness of Eqs. 13–16 can be rewritten to the discrete form. If deformation is small, only the primary parts are reserved. The normal part of the tangent stiffness matrix reads as

$$[\mathbf{K}_N] = \epsilon_N H\left(-\xi^3\right)\left[\mathbf{N}^T\right]\mathbf{n} \otimes \mathbf{n}[\mathbf{N}] \tag{20}$$

Similarly, the tangent stiffness matrix for the sticking pair is revised as

$$\left[\mathbf{K}_T^{stick}\right] = \epsilon_T\left[\mathbf{N}^T\right]\boldsymbol{\tau} \otimes \boldsymbol{\tau}[\mathbf{N}] \tag{21}$$

and the sliding pair has tangent stiffness as

$$\left[\mathbf{K}_T^{slide}\right] = \mu\epsilon_N \frac{\Delta\xi^1}{\left|\Delta\xi^1\right|}\left[\mathbf{N}^T\right]\boldsymbol{\tau} \otimes \mathbf{n}[\mathbf{N}] \tag{22}$$

Assembling of these contact stiffness $[\mathbf{K}_N]$, $\left[\mathbf{K}_T^{stick}\right]$ and $\left[\mathbf{K}_T^{slide}\right]$ into the global system tangent matrix follows standard procedures.

10 Contact Smoothing

Curved boundaries are not smooth after being discretized by linear finite elements. If structures have a rectangular shape, the corners are also not smooth. These non-smooth profiles have following issues:

a. Normal and tangential units jump from one segment to its adjacent segment.
b. Normal and tangential units have no unique value at the interaction node.
c. Unrealistically large penetration may occur at corners of the rectangle.

This non-smoothing transition of local unit vectors often triggers convergence issues. A typical example is occurrence of "chattering" when the slave node slides back and forth around an intersection on the master surface. In this paper, a Hermite interpolation method is used to smooth the contact interface as depicted in Fig. 4. Segments x_2x_3 and x_3x_4 are adjacent FE edges on the master body. Point x_a locates at αL_{23}, where $0 \leq \alpha \leq 0.5$ and L_{23} is the length of segment x_2x_3. Tangents at ends of this interpolated curve x_ax_b are defined as

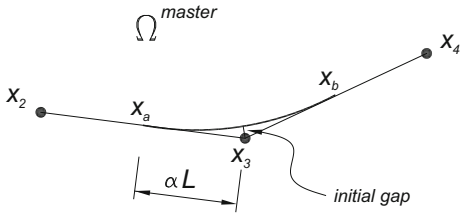

Fig. 4. Smoothing C^0 continuous boundary by Hermite interpolation

$$\begin{aligned}\frac{d\boldsymbol{x}_a}{d\xi} &= \boldsymbol{x}_3 - \boldsymbol{x}_a,\\ \frac{d\boldsymbol{x}_b}{d\xi} &= \boldsymbol{x}_b - \boldsymbol{x}_3\end{aligned} \tag{23}$$

The Hermite curve is interpolated by

$$\begin{aligned}\boldsymbol{x} = &\frac{1}{4}\left(\xi^3 - 3\xi + 2\right)\boldsymbol{x}_a + \frac{1}{4}\left(-\xi^3 + 3\xi + 2\right)\boldsymbol{x}_b + \frac{1}{4}\left(\xi^3 - \xi^2 - \xi + 1\right)\frac{d\boldsymbol{x}_a}{d\xi}\\ &+ \frac{1}{4}\left(\xi^3 + \xi^2 - \xi + 1\right)\frac{d\boldsymbol{x}_b}{d\xi}\end{aligned} \tag{24}$$

where ξ is the local coordinate of the interpolated curve $x_a x_b$.

When Hermite smoothing or other high order smoothing algorithm is used, CPP procedure should use the Newton method to find ξ_c.

11 Numerical Examples

Two examples in geotechnical engineering are presented in this section. Examples are analyzed by the FEM software package En*FEM* which was developed following implementations in this paper. Quadrilateral linear four-node elements are used for both examples.

12 Embedded Culvert Subject to Gravity Load and Unsymmetrical Ground Surcharge

The initial configuration of this example is illustrated in Fig. 5. The culvert is made up of concrete with Young's modulus 2.8×10^7 kPa. This culvert has a 180 cm outer diameter and a 144 cm inner diameter. The soil is modelled using the Mohr-Coulomb elasto-plastic material model. The coefficient of friction between the concrete and soil is 0.6. Applied loads include the gravity load and a surcharge load of 35 kPa/per unit length. Since the ground surcharge is not symmetrical, full model of culvert is used in simulation.

Two stages are considered in this analysis: stage one, with gravity load applied, and stage two, with the additional ground surcharge applied. The normal contact pressure and friction stress at the end of each stage are plotted in Figs. 6 and 7 respectively.

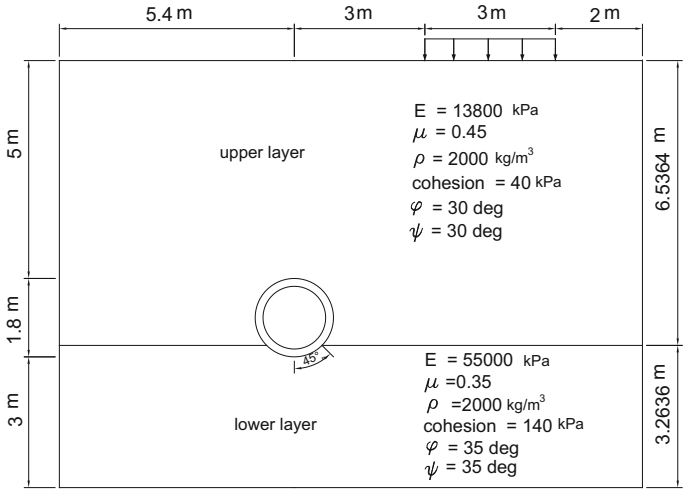

Fig. 5. Embedded culvert subject to gravity and unsymmetrical surcharge

Note that central angles start from the culvert top and rotate in the clockwise direction. Dashed orange lines are results at the end of stage 1. After the surcharge is applied, distribution of contact pressure is no more symmetric. The minimum normal pressure locates around the right interface between soft and stiff soil layers. Moment and thrust forces at the end of each stage are plotted in Figs. 8 and 9 respectively. Distributions of moment and thrust forces for each stage follow the same oscillation rhythm with shift of peaks due to the unsymmetrical total loads.

Relative sliding between soil and the culvert is very small, so that all contact pairs are sticking. No gaps are developed in this simulation.

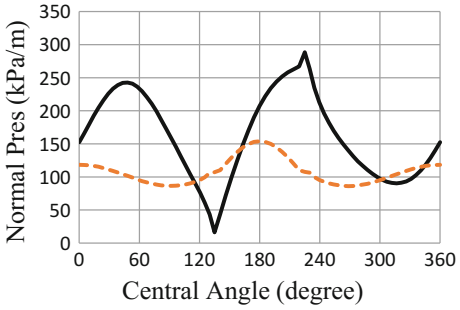

Fig. 6. Contact pressure

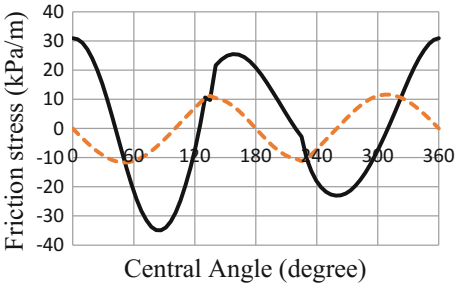

Fig. 7. Friction stress

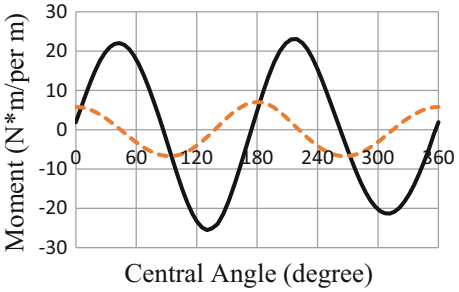

Fig. 8. Moment of culvert

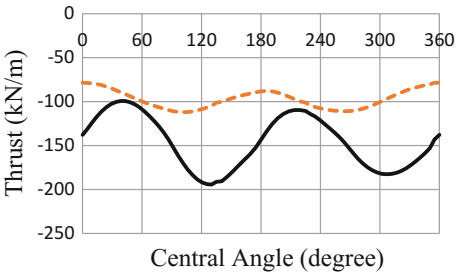

Fig. 9. Thrust of culvert

13 Stability Analysis of Slope Strengthened by a Stabilizing Pile (2D)

The second example is a 2D stability analysis of slope strengthened by a stabilizing pile. The strength reduction method is used to estimate the factor of safety against sliding. The stabilizing pile has 20 cm width and 15.6 m of length. Embedded length into the lower soil layer is about 5 m. Material properties and model geometry are shown in Fig. 10. The Mohr-Coulomb elasto-plastic material model is used for the soil.

This model has two analysis stages. Gravity load is applied during the first analysis stage followed by strength reduction stage until computations no longer converge. Calculated safety factor is about 1.412, while the safety factor without a stabilizing pile is about 1.31. Figure 11 displays the contour of horizontal displacements at failure. The deep blue zone indicates rapid soil motion to the left when slope failure occurs.

Contact pressure and friction shear stresses are plotted in Fig. 12. Approximately at depth 10 m, there is a severe jump of contact tractions. Contact statuses above this location are sliding while statuses are sticking below this location.

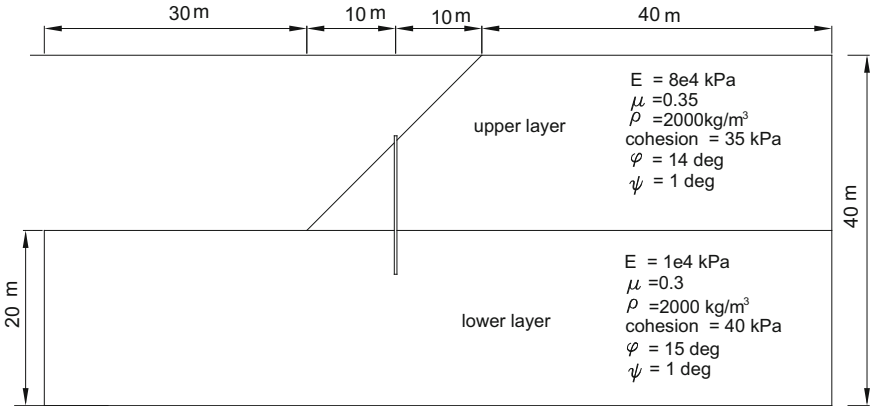

Fig. 10. Stability analysis of slope strengthened by a stabilizing pile

14 Conclusions

This paper presents implementation of computational contact analysis. Formulations in covariant form show unique advantages of being concise and easy to understand. Although non-penetration is satisfied approximately, the penalty approach provides convenient implementation and robust performance in contact problems involving finite sliding. Experience has found that local smoothing is essential if linear finite elements are used because the node-to-segment approach is sensitive to non-smooth interfaces. Two examples of 2D soil-structure interaction problems are presented.

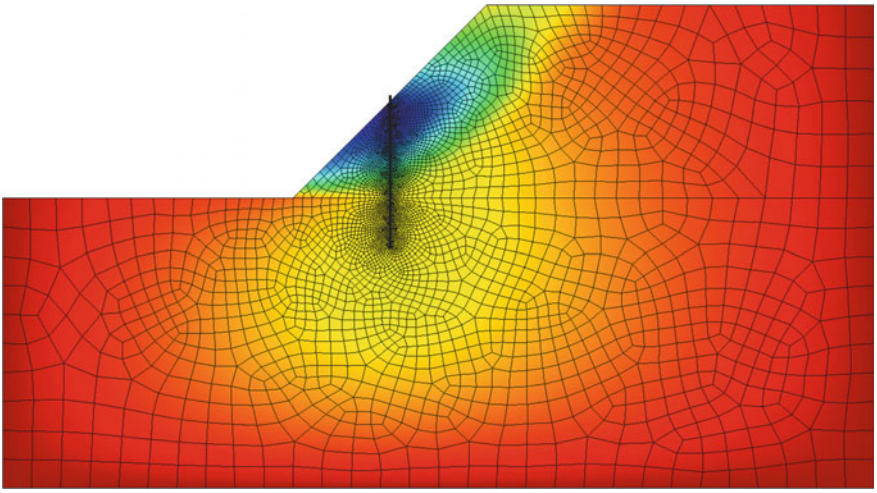

Fig. 11. Contour of horizontal displacements at slope failure

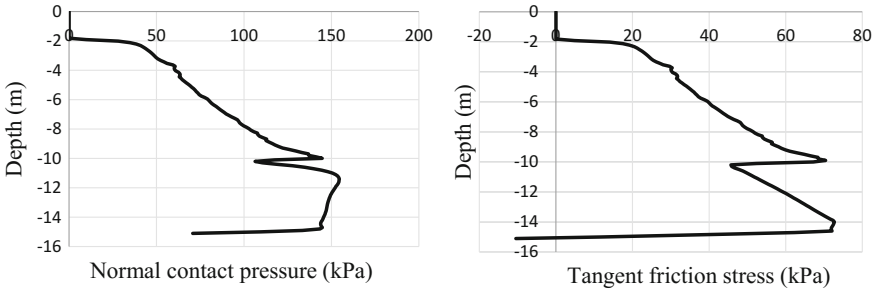

Fig. 12. Normal pressure and friction stress on right side of pile

These examples were solved using a FEM software package that was developed using the recommendations of this paper.

References

1. Goodman, R.E., Taylor, R.L., Brekke, T.L.: A model for the mechanics of jointed rock. J. Soil Mech. Found. Div. ASCE, SM3 **94**, 637–659 (1968)
2. Desai, C.S., Zaman, M.M., Lightner, J.G., Siriwardane, H.J.: Thin-layer elements for interfaces and joints. Int. J. Numer. Anal. Meth. Geomech. **8**, 19–43 (1984)
3. Francavilla, A., Zienkiwicz, O.C.: A note on numerical computation of elastic contact problems. Int. J. Numer. Meth. Eng. **9**, 913–924 (1975)
4. Hughes, T.J.R., Taylor, R.L., Sackman, J.L., Curnier, A., Kanoknukulchai, W.: A finite element method for a class of contact-impact problems. Comput. Methods Appl. Mech. Eng. **8**, 249–276 (1976)

5. Taylor, R.L., Papadopoulos, P.: On a patch test for contact problems in two dimensions, pp. 690–702. Springer, Computational Methods in Nonlinear Mechanics (1991)
6. Kikuchi, N., Oden, J.T.: Contact problems in elasticity: a study of variational inequalities and finite element methods, p. 495. SIAM, Philadelphia (1988)
7. Campos, L.T., Oden, J.T., Kikuchi, N.: A numerical analysis of a class of contact problems with friction in elastostatics. Comput. Methods Appl. Mech. Eng. **34**, 821–845 (1982)
8. Felippa, C.A.: Penalty-function interactive procedures for mixed finite elements formulations. Int. J. Numer. Mech. Eng. **22**, 267–279 (1986)
9. Konyukhov, A., Schweizerhof, K.: Computational Contact Mechanics-Geometrically Exact theory for Arbitrary Shaped Bodies. Springer, 446 p (2013)
10. Konyukhov, A., Schweizerhof, K.: A special focus on 2D formulations for contact problems using a covariant description. Int. J. Numer. Meth. Eng. **66**, 1432–1465 (2006)
11. Konyukhov, A., Izi, R.: Introduction to Computational Contact Mechanics-A Geometrical Approach. Wiley, 304 p (2015)